Mon. Not. R. Astron. Soc. **340,** 398–410 (2003)

'Fundamental Plane'-like relations from collisionless stellar dynamics: a comparison of mergers and collapses

C. C. Dantas,[1,2]★ H. V. Capelato,[2] A. L. B. Ribeiro[3]† and R. R. de Carvalho[4]‡

[1]*Departamento de Astronomia, Instituto Astronômico e Geofísico, Universidade de São Paulo, 01060-970, SP, Brazil*
[2]*Divisão de Astrofísica, INPE/MCT CP 515, 12201-970 SP, Brazil*
[3]*Departamento de Matemática Aplicada, Universidade Estadual de Campinas, 13083-970 SP, Brazil*
[4]*Observatório Nacional 20921-400 RJ, Brazil*

Accepted 2002 November 12. Received 2002 October 28; in original form 2002 April 12

ABSTRACT

We present a new set of dissipationless *N*-body simulations aiming to better understand the pure dynamical aspects of the 'Fundamental Plane' (FP) of elliptical galaxies. We have extended our previous hierarchical merger scheme by considering the Hernquist profile for the initial galaxy model. Two-component Hernquist galaxy models were also used to study the effect of massive dark haloes on the end-product characteristics. We have also performed new collapse simulations including initial spin. We found that the one-component Hernquist mergers give results similar to those found for the one-component King models, namely both were able to build up small scatter FP-like correlations with slopes consistent with what is found for the near-infrared FP of nearby galaxies. The two-component models also reproduce a FP-like correlation, but with a significantly steeper slope. This is in agreement with what has been found for elliptical galaxies at higher redshift ($0.1 < z < 0.6$). We discuss some structural properties of the simulated galaxies and their ability to build up FP-like correlations. We confirm that collapses generally do not follow a FP-like correlation regardless of the initial spin. We suggest that the evolution of gradients in the gravitational field of the merging galaxies may be the main ingredient dictating the final non-homology property of the end products.

Key words: methods: *N*-body simulations – methods: numerical – galaxies: elliptical and lenticular, cD – galaxies: fundamental parameters.

1 INTRODUCTION

The origin of the 'Fundamental Plane' relation (hereafter FP) of elliptical galaxies is still unknown, despite all the efforts made to understand it since it was discovered (Djorgovski & Davis 1987; Dressler et al. 1987).

On fundamental grounds, the simplest version of the virial theorem applied to galaxies predicts that they should form a family of objects following a simple projected relation, involving structural and kinematic variables, for instance: $r_e = C_{vir}\sigma_0^2 I_e^{-1}$. In this equation, C_{vir} is a structural-kinematic parameter, σ_0 is the central projected velocity dispersion, I_e is the average surface brightness within the effective radius in linear units and r_e is the effective radius. The coefficient C_{vir} relates physical (three-dimensional) to projected variables, such as the velocity dispersion and mass distributions. Hence, $C_{vir} \equiv C_{vir}(C_r, C_v, M/L)$ depends on kinematic (C_v) and structural (C_r) coefficients, and on the mass–luminosity ratio (M/L) of the systems (cf. Capelato, de Carvalho & Carlberg 1995, hereafter CdCC95; Dantas et al. 2002, hereafter DCdCR02).

We define a family of *homologous* galaxies as virialized systems where the kinematic and structural coefficients are simply constant for all galaxies, or may change but in a constant ratio throughout the family. If, furthermore, M/L is constant for all galaxies (or equivalently, M and L may change but stay in a constant ratio), then C_{vir} is a constant for a given homologous family.

The expression of the FP is similar to that expected from the projected virial relation but with significantly different exponents and small scatter throughout: $r_e \sim \sigma_0^A I_e^B$ (where the exponents are $A \sim 1.53$, $B \sim -0.79$, e.g. Pahre, Djorgovski & de Carvalho 1998). Thus, in the case of ellipticals, it is inferred that C_{vir} must vary monotonically among these galaxies if one is willing to retrieve the virial relation for these systems.

There are several reasonable alternatives to explain why and how C_{vir} should vary in order to explain the discrepancy between the virial theorem and the FP. One of them assumes a systematic

★E-mail: chris@das.inpe.br
†Now at: DCET, Universidade Estadual de Santa Cruz, 45650-000, Ilheus-BA, Brazil.
‡Now at: Osservatorio Astronomico di Brera, Via Brera 28, 20121, Milano, Italy.

variation of M/L with the total mass of the system, preserving homology. This would be responsible for the whole $C_{\rm vir}$ variation (e.g. Djorgovski 1988; Djogorvski & Santiago 1993; Renzini et al. 1993; Pahre & Djorgovski 1997). This dependence would be caused by systematic stellar population (e.g. mean stellar age, metallicity, etc.) variations with mass. Pahre & Djorgovski (1997) have shown that there is a dependence of the FP tilt on wavelength, namely $M/L \propto L^{\beta}$, where β varies with the photometric band (λ) in which the luminosity is measured. This means that β decreases from the B to the K band, although never reaching the homologous, virial expectations. As discussed by Pahre & Djorgovski, the trend of β with λ cannot be explained solely by either stellar population models or non-homology (see their fig. 2). They conclude that a more complete scenario to explain the FP tilt has to invoke contributions from both effects. Broken homology can be achieved both in dissipationless hierarchical merging scenarios (e.g. CdCC95) and in dissipative mergers of star-forming and gas-rich spirals, where the roles of star formation histories are emphasized (cf. Bekki 1998). A third line of reasoning for explaining the FP assumes that a more refined formulation to describe the equilibrium condition of the luminous component of the elliptical galaxies is adopting a 'two-component virial theorem', which assumes of course that ellipticals are dynamically dominated by a dark halo (Dantas et al. 2000).

In the present work, we study the origin of the FP tilt under the assumption that elliptical galaxies are more closely described as non-homologous virialized systems, with C_v and/or C_r varying monotonically (e.g. CdCC95; Hjorth & Madsen 1995; Capelato, de Carvalho & Carlberg 1997; Ciotti, Lanzoni & Renzini 1996; Busarello et al. 1997; Graham & Colless 1997; Bekki 1998). In a hierarchical galaxy formation scenario, galaxies are built-up by successive mergers of larger and larger systems. Recent observations have reinforced the idea of hierarchical merger as a reasonable mechanism for the formation of elliptical galaxies (e.g. Bender & Saglia 1999), although dissipation seems to be an important ingredient. In any case, numerical investigations of merging seem to be fundamental in understanding the scaling relations of these objects. The numerical work of CdCC95 has shown, for instance, that the FP correlations can arise naturally from objects that are formed by dissipationless hierarchical mergers of galaxies. The end products of their simulations result in a non-homologous family of objects, the peculiar non-homology mainly being determined by the parameter C_v varying systematically with the initial orbital energy of the galactic pairs. In a subsequent investigation, DCdCR02 have shown that one-component, equal-mass collapses of several different initial models and collapse factors produce nearly homologous families of objects. This result led DCdCR02 to suggest that the driving mechanism producing non-homology would be that of merging per se.

We extend the previous dissipationless numerical investigations in several aspects. First, the equilibrium models considered by CdCC95 (King spheres) do not take into consideration a central density peak. Recent studies (e.g. Gebhardt et al. 2000; Siopis et al. 2000), however, have demonstrated that the presence of a central peak (or even the presence of a central black hole) should be much more common in elliptical galaxies than previously thought. Here we consider the hierarchical merger of Hernquist models, which present a central density 'cusp'. Secondly, CdCC95 only consider one-component models. However, it is important to understand the effect of the halo in the dynamics of merging and the consequences of its influence in the equilibrium conditions of the whole system (Dantas et al. 2000). In this paper we consider the merger of two-component Hernquist models up to two generations.

One point not addressed by DCdCR02 was the initial difference in spin parameters between protogalaxies and how that can introduce non-homology into the structural properties of the final objects. In order to address this point, we investigate how the spin parameter influences the FP of the collapsed objects. However, the issue that we leave for future work is the study of two-component collapses. This is an important problem, since in the currently accepted cosmological scenarios, the luminous component collapses in the dark matter halo already virialized some time after the epoch of equality of matter and radiation energy densities. Our present goal is to establish the behaviour of only one-component collapses before analysing two-component ones, which can be studied under a more general approach such as, for instance, drawing the models from high-resolution cosmological simulations.

This paper is organized in the following way. In Section 2, we present the simulation setups and initial condition grids; in Section 3, the end products of the simulations are considered in the context of the FP space and the resulting relaxation histories. Finally, in Section 4, we discuss our main results.

2 SIMULATIONS SETUP AND DEFINITION OF CHARACTERISTIC PARAMETERS

2.1 Computer platforms and codes

The simulations were run using two C translations (cf. Dubinski 1988) of TREECODE (Barnes & Hut 1986): a non-parallel version, which was used to run less CPU time-consuming, one-component model simulations; and a parallel version, run for two-component model simulations. The computational platforms used were: (i) for the non-parallel code: Sun-Sparc workstations; Sun-Ultras (1, 2, 5, 10 and 30) and Sun E250; (ii) for the parallel code: a Silicon Graphics Origin 2000 with four processors using MPI ('message passing interface'), IRIX operational system; and a 'cluster' formed by four Pentium III, 650 MHz computers, working in parallel using LAM ('local area multicomputer') 6.3.2/MPI 2 C++, Linux.

Quadrupole correction terms, according to Dubinski (1988), were used in the force calculations for all simulations. In Table 1 we list the main parameters of the simulations setup adopted in this work. These parameters were carefully chosen in order to conform to the constraints of resolution and collisionlessness given the total number of particles used in each type of simulation (more details for the choice of parameters can be found in CdCC95 and DCdCR02). In particular, the choice of the number of particles was also based on the operational constraints owing to CPU times. Merging generally involves CPU time-consuming runs as it includes the evolution since the initial orbital phase, before the effective merger of the systems. This forced us to use a relatively small number of particles to cover a wider grid of initial conditions. These numbers, however, are well above the lower bound discussed in DCdCR02.

Table 1. Initial parameters of the codes.

Parameter	Value
θ: tolerance	0.8
ϵ: softening	
→ Non-parallel code	0.05
→ Parallel code	
Luminous component	0.07
Dark component	0.7
Δt: time integration step	0.025

2.2 Initial condition grid of the models

2.2.1 Computational units

The units used in our simulations were all set to match those of CdCC95 and DCdCR02: the mass and length units were set to $M_U \equiv 10^{10}\,\mathrm{M}_\odot$ and $L_U \equiv 1$ kpc, respectively. These values, and $G \equiv 1$, fix our time and velocity units to $T_U \equiv 4.72$ Myr and $v_U \equiv 207$ km s^{-1}, respectively.

2.2.2 The merger models

The initial equilibrium models for the merger pair were each obtained from N-particle random realizations of spheres in hydrostatic equilibrium, obeying the Hernquist profile (cf. Hernquist 1990). We considered both one- and two-component models, in equilibrium in the common potential.

The reasons for the choice of a Hernquist profile for the luminous and dark components were based on the desire to test whether models including a central density 'cusp' (in this case, the Hernquist models provided us with this characteristic) could also reproduce the results from CdCC95. Since the FP parameters refer to central (effective) quantities, the idea was to test whether the results changed sensibly or not with the inclusion of an initial 'cusp' in the models. In particular, the reasons for the adoption of the Hernquist profile for the halo (instead of, for example, a truncated isothermal profile, e.g. Walker, Mihos & Hernquist 1996) comes from the fact that the density profile behaves as $\sim r^{-1}$ at small radii resembling the Navarro, Frenk & White (1997) 'universal' profile, which results from cosmological simulations.

The Hernquist models were truncated at a specified energy cut-off: 10 per cent least bound particles of the model were eliminated. Hence, the original Hernquist one-component model had a mass of $1M_U$. The truncated model resulted in a mass of $0.9M_U$. This was also applied to the two-component models, where both the luminous and the dark component were truncated by the same factor (10 per cent): the luminous component has a mass of $0.9M_U$ and the dark component, a mass of gM_U.

We assigned to the one-component Hernquist mergers the labels: D, E and F, according to which generation they belonged to (D, first; E, second; and F, third). The total initial values for mass and number of particles of the D mergers were: $M_{\mathrm{tot,D}} = 1.8M_U$ and $N_{\mathrm{tot,D}} = 8194$, respectively (these values refer to the sum of the two initial merging models, not to one model alone).

The two-component mergers were assigned with labels Z (Z01–Z09, first generation; Z10–Z13, second generation). We chose the initial luminous (M_L) to dark (M_H) mass ratio of the initial two-component Hernquist model as $\mu_{\mathrm{init}} \equiv M_L/M_H = 0.1$ [the results of Mihos et al. (1998) favour $M_H \sim$ (4–8) $M_{\mathrm{disc+bulge}}$ for NGC 7252, suggesting our mass ratio is reasonable]. The total initial mass of the Z mergers was $M_{\mathrm{tot,Z}} = 19.8M_U$, with a total of $N_{\mathrm{tot,Z}} = 9000$ particles. Each initial two-component Hernquist model therefore has a luminous mass of 0.9 (2250 particles) and a dark mass of 9 (also 2250 particles). Note that since the number of particles per component is the same, the mass per dark matter particle is greater than that of the luminous particle by a factor of 10.

The initial ratio of the effective (half-mass) radius of dark matter to that of the luminous component was $a_H = 10a_L$. Here we briefly discuss the reasoning for choosing these ratios. Salucci & Burkert (2000) find for disc galaxies $r_0 \sim$ (4–7)R_d, where r_0 is the halo core radius of the Burkert (1995) model (r_0 is of same order as r_c, the core radius of the modified isothermal model). R_d is the disc scale radius. Noticing that the effective radius for spirals, $\langle R_\mathrm{e}^\mathrm{S}\rangle$, is approximately related to R_d by $\langle R_\mathrm{e}^\mathrm{S}\rangle \approx 1.2R_\mathrm{d}$, then $r_0 \approx$ (3.3–5.8)$\langle R_\mathrm{e}^\mathrm{S}\rangle$. Noticing also that $\langle R_\mathrm{e}^\mathrm{S}\rangle \approx R_\mathrm{e}^\mathrm{E}$ for $L = L_*$ galaxies, where R_e^E is the effective radius for giant ellipticals, and that the $R_\mathrm{e} \approx 1.8153a_L$ (cf. Hernquist 1990), where a_L is the scale radius of the Hernquist profile for the luminous component, one can infer that the results of Salucci & Burkert imply $r_0 \approx$ (6–10)a_L. Assuming a_0 is of the same order as a_H, the scale radius of the Hernquist profile for the dark matter component, there is a compatibility between our adopted values for the initial ratio ($a_H = 10a_L$) and the results by Salucci & Burkert (although their analysis was based on spiral galaxies). Gerhard et al. (2001), on the other hand, find that $r_{c,h} \approx 1.2R_\mathrm{e}$ for E0 ellipticals, where $r_{c,h}$ is the 'minimum halo model' core radius (cf. Kronawitter et al. 2000). Again, this can be translated to $r_{c,h} \approx 2.2a_L$. The correspondence between $r_{c,h}$ and a_H is not at all clear, but if they have the same order of magnitude, it would seem to imply that our value ($a_H = 10a_L$) would be somewhat higher than adequate. On the other hand, however, there are some works on the morphology and kinematics of tidal tails of merger models, where some inferences can be made concerning the halo properties by a comparison with simulations. Mihos et al. (1998), for instance, study models with ratios of mass and radius within the range of our model. They find a good fit to NGC 7252, favouring relatively compact, low-mass haloes for the progenitors of the merger. Although their results are somewhat idealistic, our models do not seem to be incompatible with what is usually adopted in the literature. However, in face of the uncertainties for a reasonable value for the effective (half-mass) radius of dark matter to that of the luminous component, we check the dependence of the FP results on the choice of this ratio. To that end, we have run two sets of nine simulations similar to the Z models, but using a more compact halo, namely: $a_H = 3a_L$ and $a_H = 5a_L$. These models are labelled Z01b–Z09b and Z01c–Z09c, respectively.

The initial merging conditions were characterized according to a generalization of a prescription described in Binney & Tremaine (1987) (cf. CdCC95). In this formulation, the initial orbit of the binary galaxy system is characterized, essentially, by the energy and angular momentum of the Keplerian orbit of two point masses equivalent to the initial galaxies. We defined the dimensionless energy and angular momentum of the orbit as

$$\hat{E} \equiv \frac{E_\mathrm{orb}}{\frac{1}{2}\mu\overline{\langle v^2\rangle}} \tag{1}$$

$$\hat{L} \equiv \frac{L_\mathrm{orb}}{\mu r_h \overline{\langle v^2\rangle}^{1/2}} \tag{2}$$

with $\overline{\langle v^2\rangle} \equiv \sqrt{\langle v_1^2\rangle\langle v_2^2\rangle}$, $\overline{r}_h \equiv \sqrt{r_{h1}r_{h2}}$, where r_{hi} ($i = 1, 2$) is the half-mass radius of the system i and μ is the reduced mass of the system. A third parameter depends only on the dynamical structure of the initial galaxies:

$$A \equiv \frac{2GM}{\overline{r}_h\overline{\langle v^2\rangle}}, \tag{3}$$

which presents a not very large variation ($\lesssim$20 per cent) among the initial models ($A \sim 17$).

The initial separation of the models was chosen as $\sim 4r_h$ for the parabolic and hyperbolic orbits, and the apocentre position for the closed orbits. These initial separations were chosen by considering that they should not be too close (implying that tidal effects would be artificially disregarded owing to the spherical symmetry of the initial models) nor too far away, so that time-consuming CPU runs were avoided.

Table 2. Mergers of Hernquist models (one component).

First generation					Second generation						Third generation					
Run	$\hat{E}$	$\hat{L}$	Sep.	$N_{\rm part}$	Run	$\hat{E}$	$\hat{L}$	Sep.	$N_{\rm part}$	Progen.	Run	$\hat{E}$	$\hat{L}$	Sep.	$N_{\rm part}$	Progen.
D01	0.0	0	15.0	8194	E1	0.0	0	16.0	15777	D01–D02	F01	0.0	0	22.0	31260	E02–E02
D02	−3.0	1	11.2	8194	E2	−2.0	1	46.4	16064	D03–D04	F02	−1.0	1	25.0	30209	E02–E05
D03	−1.0	1	33.8	8194	E3	−1.0	1	89.1	16248	D07–D08	F03	−10.0	1	15.2	28497	E02–E04
D04	−7.5	2	4.0	8194	E4	0.0	2	12.0	15416	D01–D01	F04	−7.0	2	21.8	27446	E04–E05
D05	−1.0	2	33.4	8194	E5	−3.0	0	12.0	15766	D03–D03						
D06	0.5	2	15.0	8194	E6	−0.3	0	100.0	15523	D05–D06						
D07	−6.9	3	3.4	8194												
D08	−2.8	3	10.9	8194												
D09	0.0	3	15.0	8194												
D10	−5.0	0	10.0	8194												

Table 3. Mergers of Hernquist models (two components).

First generation					Second generation					
Run	$\hat{E}$	$\hat{L}$	Sep.	$N_{\rm part}$	Run	$\hat{E}$	$\hat{L}$	Sep.	$N_{\rm part}$	Progen.
Z01	−4.0	0	70.0	9000	Z10	−2	1	207.66	17807	Z06–Z07
Z02	−4.0	1	70.0	9000	Z11	−1	1	416.04	17507	Z09–Z02
Z03	−3.0	0	70.0	9000	Z12	−1	1	416.04	17944	Z01–Z01
Z04	−3.0	1	138.2	9000	Z13	0	0	70.00	17954	Z01–Z04
Z05	−2.0	0	70.0	9000						
Z06	−2.0	1	207.6	9000						
Z07	−2.0	2	205.4	9000						
Z08	0.0	0	70.0	9000						
Z09	0.5	0	70.0	9000						
Z01b	−4.0	0	70.0	9000						
Z02b	−4.0	1	70.0	9000						
Z03b	−3.0	0	70.0	9000						
Z04b	−3.0	1	138.2	9000						
Z05b	−2.0	0	70.0	9000						
Z06b	−2.0	1	207.6	9000						
Z07b	−2.0	2	205.4	9000						
Z08b	0.0	0	70.0	9000						
Z09b	0.5	0	70.0	9000						
Z01c	−4.0	0	70.0	9000						
Z02c	−4.0	1	70.0	9000						
Z03c	−3.0	0	70.0	9000						
Z04c	−3.0	1	138.2	9000						
Z05c	−2.0	0	70.0	9000						
Z06c	−2.0	1	207.6	9000						
Z07c	−2.0	2	205.4	9000						
Z08c	0.0	0	70.0	9000						
Z09c	0.5	0	70.0	9000						

Using this grid of initial conditions, the models merged and evolved up to ∼30 'crossing times' [$T_{\rm cr} = GM^{5/2}/(2|E|)^{3/2}$], when quantities such as the half-mass radius (r_h) and the virial ratio ($\beta_v \equiv 2K/|W|$) indicated no significant variation of the resulting system ($\Delta r_h/r_h \lesssim 0.5$ per cent, and $\Delta\beta_v/\beta_v \lesssim 1$ per cent after $\sim 10T_{\rm cr}$).

In Table 2 (one-component models) and 3 (two-component models) we list the initial condition grids of the merger simulations. The two-component merger simulations using a more compact halo than the Z models (i.e. the Zb and Zc models, were $a_H = 3a_L$ and $a_H = 5a_L$, respectively) are also included in Table 3. We also list in Table 4 the simulations performed by CdCC95, including several third-generation simulations not previously published (the total number of particles for the first generation of these mergers is 8192).

Table 4. Mergers of King models (one-component, CdCC95 plus third-generation new data).

First generation			Second generation				Third generation			
Run	$\hat{E}$	$\hat{L}$	Run	$\hat{E}$	$\hat{L}$	Progen.	Run	$\hat{E}$	$\hat{L}$	Progen.
R1	0.0	0	H1	0.5	3	R17–R17	H14	−2.0	3	R6–H3
R2	−4.0	1	H2	−2.0	1	R6–R6	H15	−2.0	4	H1–H3
R3	−3.0	1	H3	−4.0	1	R17–R17	H16	0.5	4	H1–H1
R4	−2.0	1	H4	−2.0	1	R8–R8	H17	−1.77	4	H13–H13
R5	−1.0	1	H5	−2.0	1	R14–R14	H18	−3.0	3	H13–H13
R6	0.5	1	H6	−2.0	3	R2–R2	H19	−0.5	3	H10–H19
R7	−7.5	2	H7	−2.0	−3	R2–R2				
R8	−5.7	2	H8	−2.0	3	R9–R9				
R9	−1.0	2	H9	−3.0	2	R9–R9				
R10	0.0	2	H10	−3.0	−2	R9–R9				
R11	0.5	2	H11	−2.0	1	R10–R10				
R12	−7.9	3	H12	−2.0	1	R1–R1				
R13	−6.9	3	H13	0.5	2	R11–R11				
R14	−5.1	3								
R15	−2.8	3								
R16	−1.0	3								
R17	0.0	3								

2.2.3 *The collapse models*

In Table 5 we include the simulations performed by DCdCR02 for easy reference. Details of the collapse models can be found in DCdCR02. Here we give a brief summary of these collapse simulations: three different initial collapse models were used (labelled K, A and C). All the initial models have total mass $M = 20M_U$ and radius $R = 20L_U$, except the C models, which have $R = 100L_U$. The K models were constructed from 8192 Monte Carlo realizations of a spherical isotropic King model. The A models were constructed from spherical r^{-1} models of 16 384 Monte Carlo particle realizations (Aguilar & Merritt 1990). The C models were constructed according to Carpintero & Muzzio (1995), with 4096 particles. The initial velocities of these models had Gaussian profiles. All models were perturbed according to the collapse factor parameter β ($0 \lesssim \beta \lesssim 1$, where $\beta \equiv 2K_0/|W_0|$; K_0 is the initial kinetic energy and W_0 is the initial potential energy of the system). In C models, a Hubble flow assuming $H_0 = 65$ km s^{-1} Mpc^{-1} has been incorporated. We generically denoted 'cold' collapses as those resulting from $\beta \to 0$, and 'hot' collapses as those resulting from $\beta \to 1$.

We have also included two sets of collapse simulations with a range of initial solid-body rotation, not discussed in DCdCR02. We have included spins to the unperturbed, initial A model in order to

Table 5. Collapses (one-component, DCdCR02).

K models $N_{\rm part} = 8192$		A models $N_{\rm part} = 16384$		C models $N_{\rm part} = 4096$ $n = 1$		$n = 0$		$n = 2$	
$\log\beta$	Run	$\log\beta$	Run	$\log\beta$	Run	$\log\beta$	Run	$\log\beta$	Run
−4.00	K01	−4.00	A01	−3.75	C01	−3.75	C11	−3.75	C21
−3.75	K02	−3.50	A02	−3.50	C02	−3.50	C12	−3.50	C22
−3.50	K03	−3.00	A03	−3.25	C03	−3.25	C13	−3.25	C23
−3.25	K04	−2.50	A04	−3.00	C04	−3.00	C14	−3.00	C24
−3.00	K05	−2.00	A05	−2.50	C05	−2.50	C15	−2.50	C25
−2.75	K06	−1.50	A06	−2.00	C06	−2.00	C16	−2.00	C26
−2.50	K07	−1.25	A07	−1.50	C07	−1.50	C17	−1.50	C27
−2.25	K08	−1.00	A08	−1.00	C08	−1.00	C18	−1.00	C28
−2.00	K09	−0.75	A09	−0.90	C09	−0.90	C19	−0.90	C29
−1.75	K10	−0.50	A10	−0.80	C10	−0.80	C20	−0.80	C30
−1.50	K11	−4.10	A01b	−4.00	C01b				
−1.25	K12	−3.60	A02b	−3.60	C02b				
−1.00	K13	−3.40	A03b	−3.40	C03b				
−0.75	K14	−3.10	A04b	−3.10	C04b				
−0.50	K15	−2.75	A05b	−2.25	C06b				
−0.25	K16	−2.25	A06b	−1.75	C07b				
−0.01	K17	−1.75	A07b	−1.25	C08b				
		−1.25	A08b	−0.25	C09b				
		−0.95	A09b	−0.10	C10b				
		−0.85	A10b						
		−0.25	A11						
		−0.10	A12						

study their effects on the final systems. The reason to focus on the A models is because these collapses spread in the FP space, contrary to the K models. Although the C models are more 'realistic' (they evolve from small perturbations in a Hubble expansion), because of being dynamically more complex we have avoided them our analysis of the spin effect on the FP (see details in DCdCR02).

The method we assume here is inspired by that of Wilkinson & James (1982). We have given a solid-body angular velocity, ω, to each particle of the unperturbed A model. The value of ω was chosen such that the resulting total kinetic energy after including the spin was a fraction γ greater than the initial total kinetic energy (i.e. without the rotational motion). In other words, $\gamma = |K_{\rm prog} - K_{\rm prog,spin}|/K_{\rm prog}$. For the first set of collapse simulations with spin, which we label as AS1 models, the rotational perturbation chosen was small, $\gamma \sim 5$ per cent. The total velocity squared of each particle was then reduced by a range of β factors, producing nine spin models with different collapse factors. These collapses can be directly compared with the A collapses studied by DCdCR02. For the second set of models, γ was chosen in order to impose a maximum perturbation to the A progenitor such that, after reducing the velocity field by the 'hottest' perturbation we are considering (namely $\log\beta = -0.01$), the resulting model was barely able to collapse (the total binding energy was ~ -0.007). The value of the perturbation in this case was $\gamma \sim 38$ per cent. The perturbed progenitor was 'cooled' by the same β factors as the AS1 models. This second set of models was labelled as AS3 models. These new collapse simulations are listed in Table 6.

Note that the structure (namely potential energy) of the A models used here to construct the spin models did not allow the inclusion of a higher initial spin than that of the AS3–09 ($\log\beta = -0.01$) model without disrupting the system (namely expanding it instead of making it collapse). Higher spin rates could have been used, but that would imply changing the structure of the progenitor by, for example, reconfiguring the positions of the particles (namely by decreasing the gravitational radius of the system) or increasing the total mass. That would change the structure of the progenitor considerably and would not allow a direct comparison with the collapse models of DCdCR02. Hence, these collapses with spin just represent models where an initial rotational 'perturbation' was applied to the system. This allowed us to keep the same initial structure of the progenitor of the A models, used by DCdCR02, and still make the resulting model collapse according to the β factor.

Table 6. Collapses (the 'A' model progenitor with initial spin).

AS1 models $N_{\rm part} = 16384$, $\gamma = 5$ per cent		AS3 models $N_{\rm part} = 16384$, $\gamma = 38$ per cent	
$\log\beta$	Run	$\log\beta$	Run
−4.00	AS1–01	−4.00	AS3–01
−3.50	AS1–02	−3.50	AS3–02
−3.00	AS1–03	−3.00	AS3–03
−2.50	AS1–04	−2.50	AS3–04
−2.00	AS1–05	−2.00	AS3–05
−1.50	AS1–06	−1.50	AS3–06
−1.00	AS1–07	−1.00	AS3–07
−0.50	AS1–08	−0.50	AS3–08
−0.01	AS1–09	−0.01	AS3–09

3 THE FUNDAMENTAL PLANE OF END PRODUCTS

3.1 The FP space

We follow the method given by CdCC95 to compute the characteristic FP variables ($r_{\rm e}$, $\mu_{\rm e} \equiv -2.5\log I_{\rm e}$ and σ_0) of the simulated models. The variables σ_0 and $\mu_{\rm e}$ were combined on the vertical axis

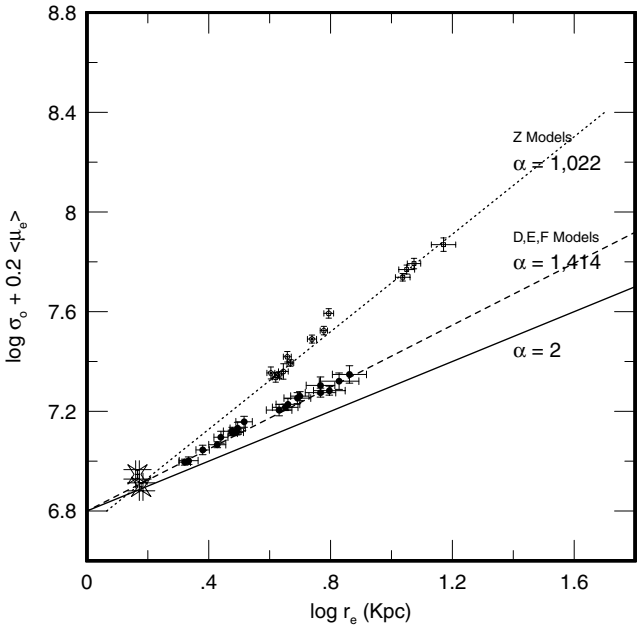

Figure 1. Results of the merger simulations in terms of the FP parameters. In the case of two-component models, only the luminous component is presented. The stellar symbol represents the progenitor. The continuous line represent the prediction of the virial theorem for homologous systems.

according to the usual representation of the FP projected on to the Cartesian plane $\log r_e \times \log \sigma_o + \beta \mu_e$. In all the cases the 3-variate best-fitting solutions for a plane gave $\beta = 0.2$ to within 10 per cent, so we decided to keep this coefficient fixed at 0.2 in order to find the orthogonal least-squares solutions for the other coefficients, namely the slope α (the FP 'tilt'), and the intercept of the fitted plane.

Before analysing the final simulated models in the FP space, however, it is worth commenting that they reproduce the general structural characteristics of elliptical galaxies, e.g. projected triaxialities (from E0 to E5 elliptical objects) and surface density profiles (following the Sérsic law). A detailed discussion on the structural properties of the simulated models is given in Dantas (2001).

In Fig. 1 we present the characteristic FP parameters of the objects resulting from the merging of one- (D, E and F mergers) and two- (Z mergers) component models. In the case of two-component models, the data shown in this figure are relative to the luminous component. The best-fitting values for the FP slope (α) found for these simulations are indicated in the figures. The continuous line ($\alpha = 2$) represent the prediction of the virial theorem for homologous, constant M/L, systems. In Table 7, we present the results of the best-fitting values for the data discussed here and the results obtained by CdCC95 and DCRdC02. The results indicate that one-component Hernquist mergers (D, E, F) also reproduce the FP tilt of the elliptical galaxies reasonably, consistent with the results obtained with the King models of CdCC95. That is, for both cases, the FP slopes are consistent, within the errors, with that observed for infrared FP of nearby galaxies, i.e. $\alpha = 1.53 \pm 0.08$ (Pahre et al. 1998).

On the other hand, the luminous/baryonic objects resulting from the two-component mergers form a family with a steeper relation in comparison with one-component mergers. (It is interesting to note that if we consider an equivalent to the FP space but for the dark haloes of these merger remnants, we find that they constitute an approximately homologous family of objects, as indicated by the

Table 7. PF best-fitting values.

Model	$\alpha \pm \delta\alpha$	$N_{\rm fit}$
One-component models:		
D, E, F mergers	$\alpha = 1.414 \pm 0.132$	20
King (CdCC95) mergers	$\alpha = 1.36 \pm 0.08$	17
K collapses	No fit: cluster of data points	17
C collapses:		
$n = 0$	$\alpha = 2.070 \pm 0.123$	10
$n = 1$	$\alpha = 2.161 \pm 0.087$	19
$n = 2$	$\alpha = 2.033 \pm 0.342$	10
A collapses	$\alpha = 1.954 \pm 0.123$	22
AS1 collapses (all)	$\alpha = 2.306 \pm 0.250$	9
AS1 collapses (removing AS1–09)	$\alpha = 2.204 \pm 0.158$	8
AS3 collapses (all)	$\alpha = 2.190 \pm 0.349$	9
AS3 collapses (removing AS3–09)	$\alpha = 1.966 \pm 0.270$	8
Two-component models:		
Z models ($a_H = 10a_L$):		
Luminous comp.	$\alpha = 1.022 \pm 0.046$	13
Dark comp.	$\alpha = 1.872 \pm 0.152$	13
Both components	$\alpha = 1.176 \pm 0.070$	13
Zb models ($a_H = 3a_L$):		
Luminous comp.	$\alpha = 1.004 \pm 0.123$	9
Zc models ($a_H = 5a_L$):		
Luminous comp.	$\alpha = 1.017 \pm 0.105$	9

value $\alpha = 1.872$, in Table 7.) In order to test the effects of a more compact halo on these results, we ran two groups of two-component Hernquist mergers with different ratios for the halo to luminous radius (as discussed in Section 2.2.2). Unlike the Z models, these runs were not followed for subsequent (namely second, etc.) generations because of CPU time limitations. In Fig. 2, we show how these more compact halo mergers distribute in the FP space. The arrows over the dotted lines in that figure represent the range occupied by the first-generation Z models ($a_H/a_L = 10$), for comparison. It is interesting to note that the luminous component of the most compact halo models (Zb models), with most negative $E_{\rm orb}$ values, tend to cluster in the FP space in a similar manner to the *K* collapses. All other models tend to spread out sensibly along a FP-like relation. Also, the luminous body of these models (Zb and ZC models) tend

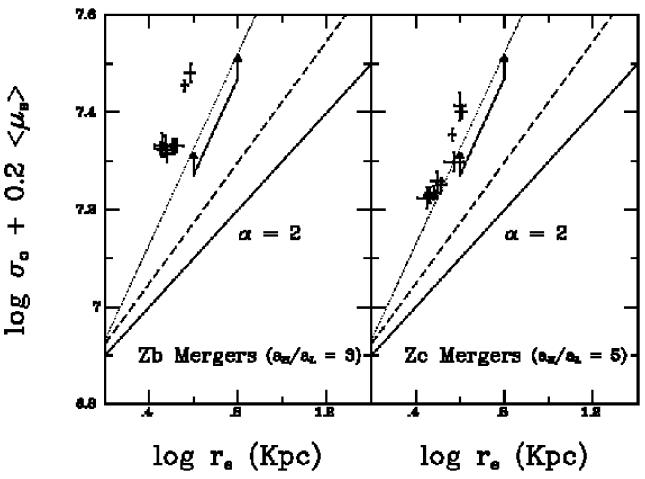

Figure 2. Results for the luminous component of the Hernquist merger simulations, using more compact haloes. Left-hand panel, Zb mergers; right-hand panel, Zc mergers. The three lines on these panels are reproductions of the fits shown in Fig. 1, for comparison. In particular, the solid line is the prediction of the virial theorem for homologous systems. The arrows over the dotted line represent the range occupied by the first-generation Z models ($a_H/a_L = 10$), for comparison.

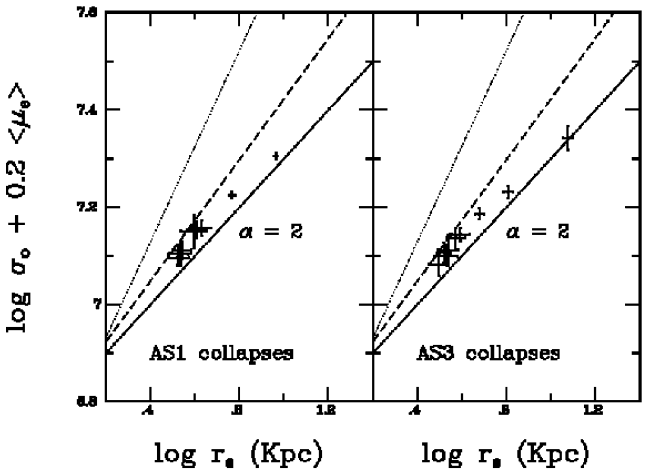

Figure 3. Results of the collapse simulations with initial spin in terms of the FP parameters. Left-hand panel, AS1 collapses, constructed from the progenitor of the 'A' models. This progenitor received a solid-body rotation resulting in a ∼5 per cent perturbation to the initial total kinetic energy of the system, and then 'cooled' by a range of β factors. Right-hand panel, AS3 models, produced in a similar manner to the AS1 collapses, but receiving a larger initial rotational perturbation (∼38 per cent). The three lines on these panels are reproductions of the fits shown in Fig. 1, for comparison. In particular, the solid line is the prediction of the virial theorem for homologous systems.

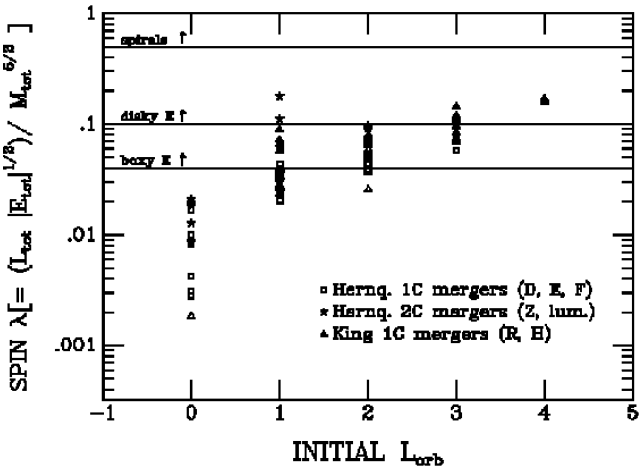

Figure 4. Distribution of the spin of the mergers as a function of the initial orbital angular momentum of the pre-merger pair.

to settle into systematically lower values of r_e and at higher values of y ($\equiv \log\sigma_0 + 0.2\langle\mu_e\rangle$) than the Z models ($a_H/a_L = 10$). The FP 'tilts' of these models suggest a marginally steeper 'tilt' than the Z models.

As already mentioned, we have performed two groups (AS1 and AS3 models) of collapse simulations with initial spin in order to verify the effects of the inclusion of rotation on the results by DCdCR02, where evidence for homology were found for pure collapses. The resulting FP 'tilts' for both groups ($\alpha_{AS1} = 2.204 \pm 0.158$; $\alpha_{AS3} = 2.306 \pm 0.250$) suggests that the resulting models are slightly non-homologous, but in the *opposite* (namely $\alpha > 2$) sense from the observed FP 'tilt' of elliptical galaxies (cf. Fig. 3).

All of these new collapse models evolved for more than 2 Gyr ($\sim 30 T_{cr}$), however, the 'hottest' models (namely AS1–09 and AS3–09, both with initial $\log 2K/|W| = -0.01$) still presented a virial ratio oscillating around $2K/W \sim -1.4$ by that time. These 'hottest' models seem to evolve very slowly and still did not reach complete virial equilibrium after 2 Gyr, whereas all the other models were already well virialized. Removing these 'hottest' collapse models results in $\alpha_{AS1-0.01} = 1.966 \pm 0.270$ and $\alpha_{AS3-0.01} = 2.190 \pm 0.349$, which are compatible with homology.

Although we cover a reasonable range of β values, it is not clear whether the inclusion of more intermediate β collapses would necessarily improve the statistics (i.e. decrease the error bar of the fit), since the 'coldest' models tend to cluster in the FP space. On the other hand, the inclusion of 'hotter' collapses would only exacerbate the observed 'inverted' (namely $\alpha > 2$) non-homology. These results seems to indicate that an initial spin is not sufficient to produce non-homology, at least of the same nature as mergers.

3.2 Spin analysis

In this section we briefly analyse how the final spin of the models depends on the initial condition. We parametrize the spin by the dimensionless quantity λ, defined by (cf. Peebles 1971)

$$\lambda = \frac{L|E|^{1/2}}{GM^{5/2}}, \tag{4}$$

where L is the total angular momentum of the system about its barycentre, E is the total energy of the system and M is the total mass (as already mentioned, $G = 1$).

Fig. 4 shows how the spin of the mergers distributed as a function of the initial orbital angular momentum of the pre-merger pair. First, it can be seen that indeed there is a transfer of L_{orb} to the final spin of the merger, since higher L_{orb} values produce systematically higher final spins. Secondly, intermediate L_{orb} values ($1 < L_{orb} < 3$) produce objects with spins compatible with boxy ellipticals. We note, however, that the position of the merger products on the FP depends very little on L_{orb} (cf. CDCC95). In other words, $L_{orb} = 3$ mergers could perfectly well be produced from $L_{orb} = 0$ mergers, and the final products would have approximately the same positions on the FP.

Fig. 5 plots both mergers and collapses as a function of the initial conditions E_{orb} and β, respectively. It can be seen that mergers from a wide range of E_{orb} values are able to produce objects in the observed range of ellipticals, as opposed to collapses, which fail in this respect. It is interesting to note that 'colder' collapses reach a higher degree of final spin than the 'hottest' ones. This seems to

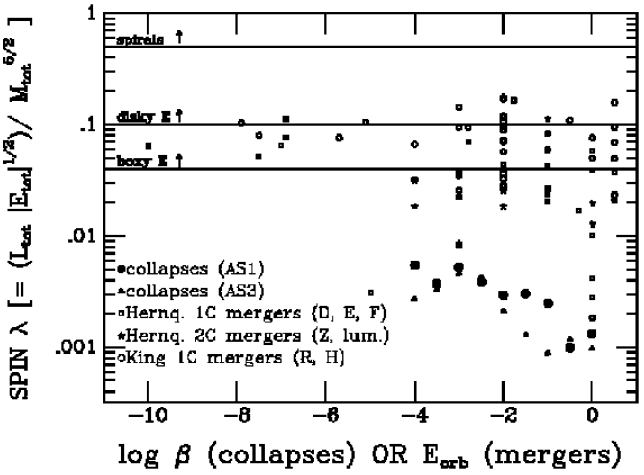

Figure 5. Distribution of the spin of collapses and mergers as a function of the initial collapse factor (β) and orbital energy (E_{orb}), respectively.

imply that the initial rotational perturbations are amplified in the 'coldest' collapses. Yet, as we have seen, these 'colder' objects still manage to become approximately homologous (see the fits for AS1–09 and AS3–09 sequences in Table 7). Evidently, these results must be interpreted with caution, since we did not reconfigure the initial structure of the progenitor in order to include higher initial spins.

3.3 The virial coefficients

We use another diagnostics for testing homology on the final simulated objects. A good quantitative measure in this case is the direct computation of the kinematic–structural or virial coefficients (C_r, C_v), as described in CdCC95 and DCdCR02:

$$C_r \equiv r_{\rm G}/r_{\rm e} \tag{5}$$

and

$$C_v \equiv \langle v^2\rangle \Big/ \sigma_0^2, \tag{6}$$

where $r_{\rm e}$ is the effective radius (the radius that defines a sphere containing half of the total luminosity of the system): $L(<r_{\rm e}) = L_{\rm tot}/2$. σ_0 is the central projected velocity dispersion and $r_{\rm G}$ is the gravitational radius, defined by $r_{\rm G} \equiv GM^2/|W|$, where W is the total potential energy of the system. $I_{\rm e} \equiv L(<r_{\rm e})/\pi {r_{\rm e}}^2$ is the mean surface brightness within $r_{\rm e}$, in linear units. Then, $I_{\rm e} = C_I(\frac{M/2}{\pi r_{\rm e}^2})$, with $C_I \equiv (M/L)^{-1}$. Inserting the above equations into the virial relation ($\langle v^2\rangle = GM/r_{\rm G}$), we find that $r_{\rm e} = C_{\rm vir}\sigma_0^2 I_{\rm e}^{-1}$, where

$$C_{\rm vir} \equiv \frac{C_r C_v}{2\pi G C_I}. \tag{7}$$

Since, by construction, C_I (namely M/L) is constant among the models, the computation of C_r and C_v directly gives the measure of non-homology among the simulated models. Note that for two-component systems, $r_{\rm G}$ and $\langle v^2\rangle$ are calculated from, respectively, the total potential and kinetic energy of the system. Values of σ_0 and $r_{\rm e}$ correspond, however, only to the visible/baryonic matter. As already pointed out, non-homologous objects are those where the kinematic–structural coefficients assume different values for each object. The results are presented in Fig. 6, where we plot the coefficients as a function of the initial conditions.

First, we find that the structural coefficients, C_r, attain different ranges of values for one- and two-component models: for one-component mergers, $2.5 \lesssim C_r \lesssim 3.5$; whereas for two-component mergers, $8 \lesssim C_r \lesssim 15$. This difference is caused by the presence of the massive halo in the two-component models, which pushes the gravitational radius to larger values, as compared with the one-component systems. This increase of $r_{\rm G}$ cannot, however, be compensated by $r_{\rm e}$, which depends only on the structure of the luminous core. The kinematic coefficients, C_v, on the other hand, show similar ranges for both types of mergers. The product C_rC_v (cf. the upper panel of Fig. 6) therefore attains larger values for two-component models than for one-component ones.

A more relevant aspect of Fig. 6 is the fact that the kinematic–structural coefficients vary in a systematic manner as a function of the initial orbital energy of the merging models, which is in agreement with the results found by CdCC95. This behaviour seems to be an important feature distinguishing mergers from collapses. Indeed, collapses as a whole are approximately homologous objects, although some distinctions between 'cold' and 'hot' collapses are found (a detailed discussion of collapses can be found in DCdCR02). There seems to be no correlation with the orbital angular momentum, as can be seen from an inspection of Fig. 6. On the other hand,

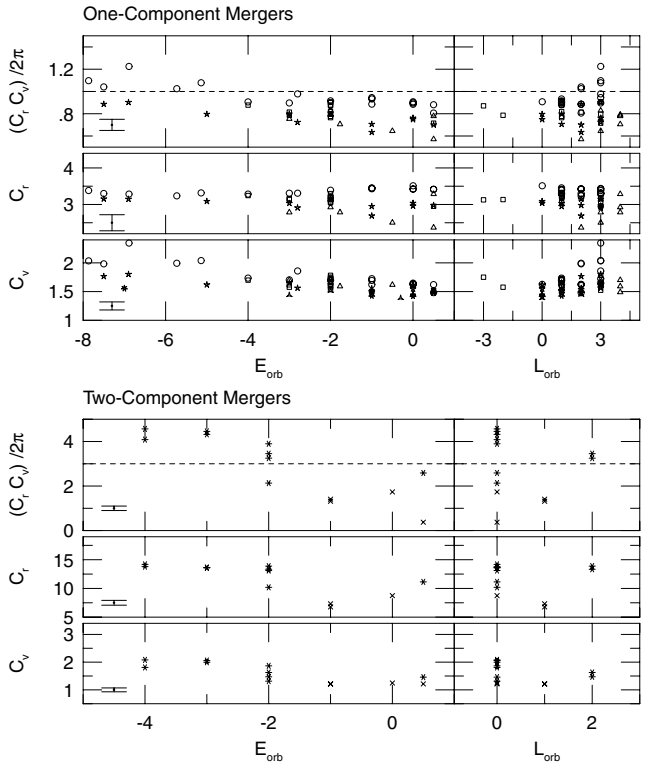

Figure 6. Ratio of the virial coefficients $C_{\rm vir}$, C_r and C_v as a function of the initial conditions. The symbols represent: five-point stars for the D models; three-point stars for the E models; seven-point stars for the E models; six-point asterisks for the Z models (first generation); four-point asterisks the for Z models (second generation); open circles for the King models (first generation); open squares for the King models (second generation); and open triangles for the King models (third generation). A dashed horizontal line is indicated and represents an arbitrary homologous family of objects for comparison.

it can be seen that the deviation from homology is more accentuated for two-component mergers: if we take the total fractional difference of $y(E_{\rm orb}) \equiv (C_rC_v)/2\pi$, $\delta y \equiv |y(E_{\rm orb\,max}) - y(E_{\rm orb\,min})|/y(E_{\rm orb\,max})$, we find $\delta y \sim 0.9$ for two-component mergers, whereas $\delta y \sim 0.5$ for one-component models (δy is $\sim$0 for homologous objects). This quantity therefore reproduces the deviation from homology as pictured in the FP space (cf. Fig. 1), with the advantage that it is possible to trace the source of non-homology from the corresponding fractional differences of the C_r and the C_v coefficients separately. For one-component mergers, $\delta(C_r) \sim 0.14$, $\delta(C_v) \sim 0.25$; for two-component mergers, $\delta(C_r) \sim 0.38$, $\delta(C_v) \sim 0.42$. Therefore, for one-component mergers, C_v contributes more to the non-homology than C_r, a feature that can be seen clearly from an inspection of Fig. 6.

3.4 The ratio of 'central' to 'envelope' kinetic energies

The results of the previous section demonstrate that the (central) non-homology effect that characterizes our merger simulations has a predominantly kinematic origin. Now we will analyse the behaviour of the total kinetic energy *interior* to a given radius as compared with the corresponding kinetic energies *exterior* to that radius. In other words, if we call $K_{\rm tot}(<r)$ the 'central' kinetic energy of the system and $K_{\rm tot}(>r)$ the kinetic energy of its 'envelope', then a measure of the ratio of these quantities, $K_x \equiv K_{\rm tot}(r > xr_h)/K_{\rm tot}$ ($r < xr_h$), *normalized to its progenitor value*, should reveal, at least

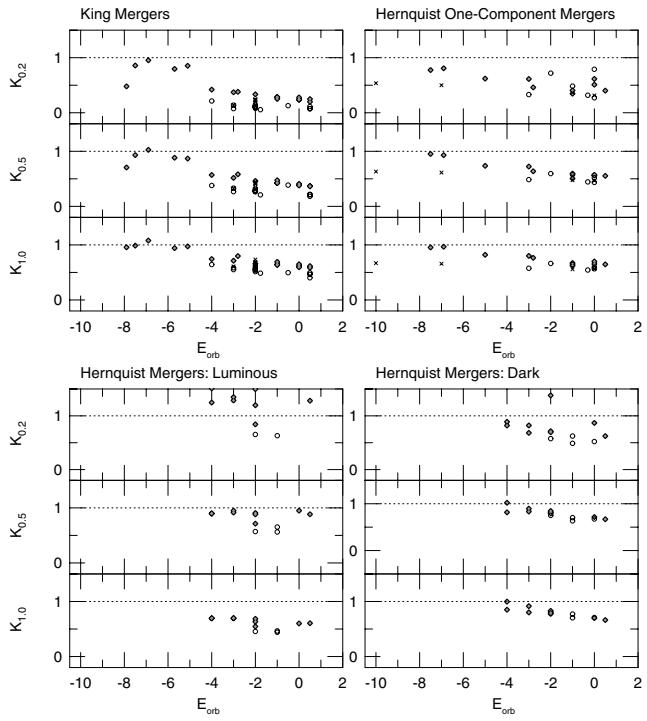

Figure 7. Ratio of the kinetic energies exterior and interior to three distinct radii: $0.2r_h$, $0.5r_h$ and $1r_h$ [notation of the figure: $K_x \equiv K_{\rm tot}(r > xr_h)/K_{\rm tot}(r < xr_h)$, normalized by the corresponding value of the progenitor (unperturbed model)], as a function of the initial conditions. The dashed line indicates that the value of $K_x = 1$. Diamonds represent the first generation, circles the second generation and crosses the third generation.

in a gross sense, the effects of the relaxation process. This process will therefore be viewed as alterations of the kinetic energies of the more gravitationally bound ('central') particles against the less bound ones ('envelope'). Thus if $K_x = 1$ then the end product model presents the stratification of kinetic energies similar to the progenitor model. If, however, $K_x < 1$ then the 'central' particles are 'hotter' than the 'envelope', *as compared with the progenitor*.

We analysed the kinetic energy ratio, K_x, as a function of the initial conditions (the collapse factor or orbital energies, for the merger), for three different radii ($x = 0.2$, 0.5 and 1). The results are shown in Fig. 7 for the mergers models and in Fig. 8 for the collapse models.

Most collapse models present $K_x < 1$ for any x. The 'hottest' K collapses, on the other hand, approach $K_x \to 1$. In other words, the values for K_x do not change with the initial collapse factor (β), except for the 'hottest' K collapses. Moreover, the values for K_x are similar among different models, except, possibly, the C models which seem more noisy than the others. For larger x, all the collapse models have $K_x \to 1$. The general trend is that the collapse models are centrally 'hotter' than the corresponding progenitor, *independently of the initial* β (except for βs very close to 1) and the initial model used.

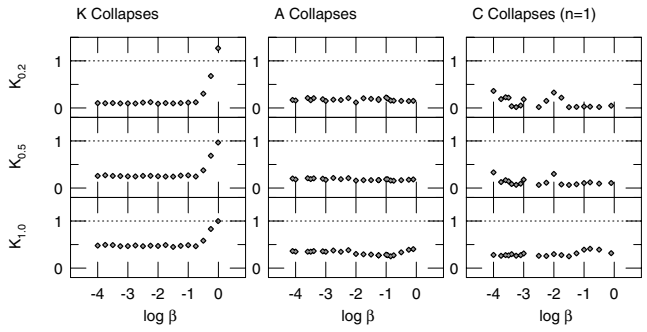

Figure 8. The same as in the previous figure, but for collapses.

The stratification of kinetic energies in the case of mergers is not similar to the collapses. For mergers, it is clear that K_x *is a systematic function of the initial orbital energy of the pairs*. In other words, for mergers with more negative initial orbital energies $K_x \to 1$, show no difference from their progenitors, whereas those with less negative energies deviate more from the progenitor, *and in a systematic way*, towards $K_x < 1$. The magnitude of the deviation from $K_x = 1$ also depends on the merging models: for instance, it is greater for the King models, intermediate for the Hernquist one-component models and smaller for the Hernquist two-component models. It also seems to increase slightly for increasing merger generations. There are also examples where $K_x > 1$ (some Hernquist two-component models, with $x = 0.2$). In other words, the behaviour of K_x for mergers seems to be more complex than collapses and shows a clear systematic dependence on the initial orbital energy of the pairs, in the same sense that the virial coefficients depend systematically on $E_{\rm orb}$.

In the case of mergers, the systematic dependence of K_x on $E_{\rm orb}$ begins to flatten and tends to be erased for sufficiently large values of x. This, in fact, shows that the merger models tend to a similar stratification of the 'central' and 'envelope' kinetic energies at sufficiently large radius. In other words, the different K_x values among the merger models are not only a function of the initial orbital energy but is also a function of x, so the correlation $K_x \times E_{\rm orb}$ is stronger at the very centre of the models and tends to disappear at sufficiently large radii. This therefore shows that the effect is intimately related to the central parts of the system.

Our detailed description of the ratio of kinetic energy behaviour among models, as given in this section, seems to reinforce the idea that the non-homology in mergers is a central effect ruled by how the particles gain kinetic energy during the merger. In other words, the non-homology seems to have a dynamical origin that is not present in simple collapses.

In the following, we focus on the analysis of the relaxation history of both mergers and collapses, which may help us to find clues to understanding the dynamical processes that are at the origin of the non-homology of mergers.

3.5 Relaxation histories

3.5.1 Evolution of the virial ratio $2K/W$

In order to trace a measure of the fluctuations of the gravitational potential on its way to equilibrium, we compared the behaviour of the virial ratio $2K/W$ (measured for the whole system, including escapers) during the evolution of different and representative types of models, namely: a 'cold' (A01 model, $\log\beta = -4$) and a 'hot' (A09 model, $\log\beta = -0.75$) collapse; against a 'rapid' (D10 model, $E_{\rm orb} = -5$, $L_{\rm orb} = 0$) and a 'slow' (D9 model, $E_{\rm orb} = 0$, $L_{\rm orb} = 3$) one-component merger. Fig. 9 shows the behaviour of these representative models. Note that some models do not stabilize around $2K/W = -1$, as would be expected for a virialized model. This arises from the fact that we are measuring the virial coefficient using the complete particle data, including particles with positive energies that have escaped the system. More 'violent' relaxations produce more escapers, and the resulting virial ratio stabilizes around some other value slightly different from -1.

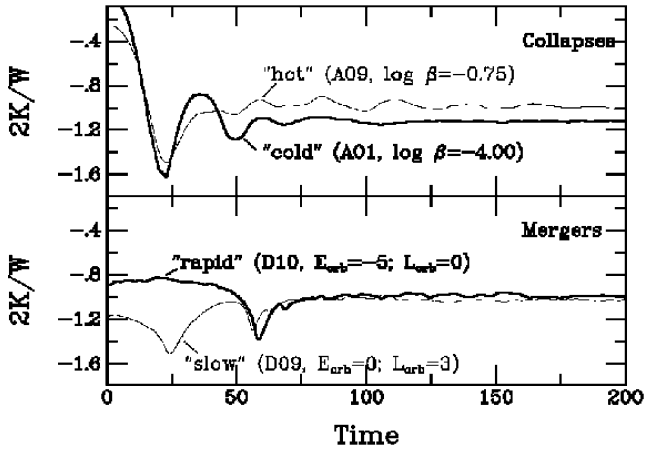

Figure 9. The behaviour of the virial ratio $2K/W$ during the evolution of different and representative types of models. Upper panel, collapses; lower panel, mergers.

We note that the most rapidly merging system suffers only one major fluctuation of $2K/W$, subsequently rapidly reaching equilibrium. The slower merger shows that $2K/W$ varies over large periods during the first moments of the evolution (in other words, it does not show a unique abrupt change in $2K/W$, but rather two or more large-periodic fluctuations before reaching equilibrium). Collapses, regardless of being 'cold' or 'hot' show one large initial fluctuation amplitude in $2K/W$. Interestingly, the subsequent evolution seems to be different: the 'cold' collapse still experiences one more relatively significant fluctuation of $2K/W$ before reaching equilibrium. The 'hot' collapse, on the other hand, still shows a persistent, although low-amplitude, fluctuation of $2K/W$ for some time, when the 'colder' collapse is comparatively well stabilized.

3.5.2 The 'Kandrup' effect

In order to understand the dynamical behaviour presented by the simulated models, we apply a diagnostic advocated by Kandrup, Mahon & Smith (1993). The merging of stellar systems occurs because of a transfer of the orbital energy to the particles of the stellar systems in question. The mechanisms through which this occurs are the tidal interactions, which increase the internal energy of the systems at the expense of their orbital energy. The question here concerns the relation of this mechanism with the central non-homology of the simulated mergers.

During the evolution of the system, the energy of the particles is not, in general, conserved, even in a 'coarse-grained' sense [namely through the distribution $N(E)$; for a discussion on the importance of this distribution for stellar systems, see Binney (1982)]. Kandrup et al. studied the distribution of the energy of the particles in systems resulting from collisions (without the formation of a final single object) and merging of two galaxies. These authors found that *there is* a 'coarse-grained' sense in which the *ordering* of the mean energy of given collections of particles is unaltered, even though $N(E)$ may vary substantially. In this section, we revisit the question raised by Kandrup et al. and try to connect this fact with the behaviour of the simulated systems in the context of the FP. Note that their conclusions were based on only two simulations of collisions, with only one merger, and two collapses. Here we use a much larger set of simulations and initial conditions, and a larger number of particles compared with the models used by Kandrup et al. We will not consider the time evolution of mean energies, as Kandrup et al. did, but only the initial and final values for the mean energy of the given collections of particles. We discuss their diagnostic further below.

The method may be considered as a 'Lagrangian' approach to the analysis of how the energy of the particles changes because of the relaxation process. The particles of the *initial* models have been sorted according to their binding energies and the models were partitioned into five bins of equal numbers of particles (a finer partitioning with 10 bins produced essentially the same results). For each of these bins, the mean energy was calculated and the bins ranked with the first one initially containing the most bound particles (most negative mean energy) whereas the fifth contains the least bound ones (least negative mean energy). The mean energy of these collections of particles were then recalculated at the end of the runs and compared with their initial values. We have limited our analysis for the first generation of mergers. In the case of mergers with equal $E_{\rm orb}$ values, we have included only the model with lower $L_{\rm orb}$. The results of these comparison are displayed in Figs 10 and 11.

We found that, except for some of the C cases, collapses preserve the ordering of the mean energies per bin entirely. These results confirm the findings of Kandrup et al. Moreover, the mean energies per bin that changed more in this case were those corresponding to the most bound bins (1, 2, 3, etc.). The central potential becomes

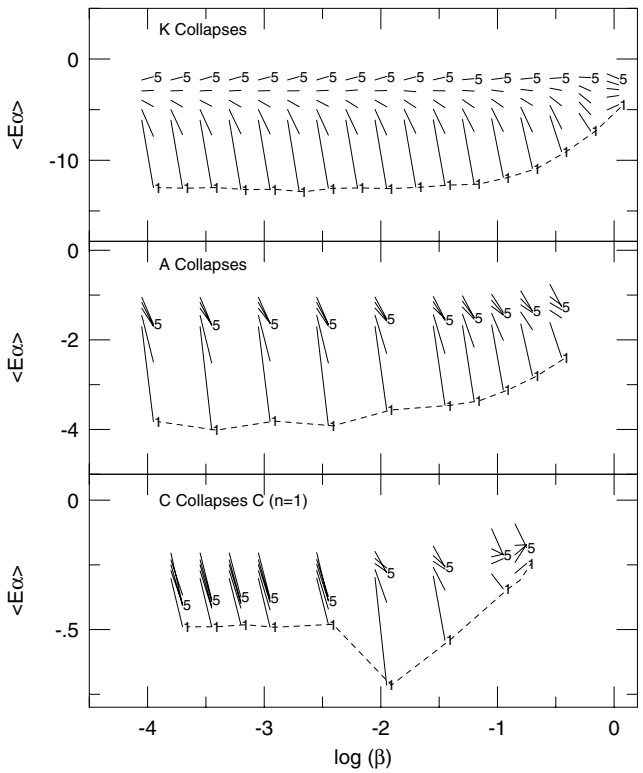

Figure 10. Energy means of five equal number collections of particles, ordered according to their initial mean binding energies. The initial and final mean binding energy values are connected by a line segment (left extreme, initial mean value; right extreme, final value), centred in the initial condition of each model. 'Bin numbers' are indicated in the figure: bin 1 refers to the most bound particles and successively to bin 5, which refers to the most weakly bound particles. The values for the final mean binding energy of the initially most bound bin (1) are connected with a dashed line, illustrating how it changes as a function of the initial condition. The models shown are collapses.

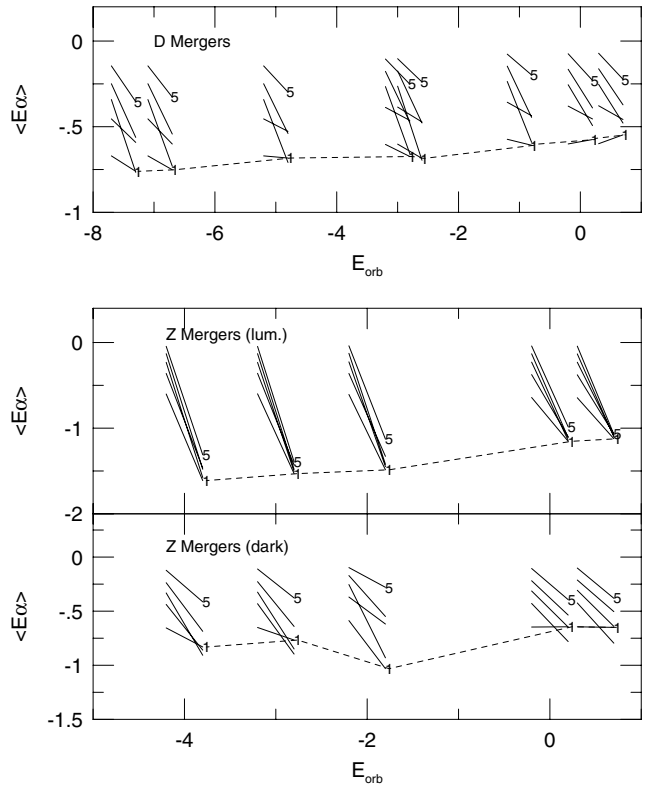

Figure 11. The same as in the previous figure, but for first-generation mergers. In the case of mergers with equal $E_{\rm orb}$ values, we have included in the figure only the model with lower $L_{\rm orb}$.

deeper after the collapse, and the particles initially more bound to the system tend to lose energy, becoming even more tied. This effect is also a function of the collapse factor β, as can be seen by the dashed line in the figure, which connects the most bound bin (1), illustrating how this bin changes as a function of the initial condition. In the case of A collapses, the mean energies representing the three less bound bins converge to similar final values, whereas the two most strongly bound bins reach even more negative mean values. This behaviour indicate that collapses tend to produce core–halo structures. In the case of C collapses, the mean energies change considerably and chaotically. Recall that these models contain a Hubble flux that may favour the growth of perturbations embedded in these models, adding some complexity in the evolution of the mean energy of these distinct collections of particles.

In the case of mergers (one- and two-component models), the preservation of the ordering of the mean energies per bin is not as good as in the case of collapses. For the D models (Hernquist one-component models), the initially most bound particles will remain as the most bound ones after the relaxation process. However, it can be seen that bin 3 actually crosses bin 2 and reaches values corresponding to bin 1. In the case of two-component models, the luminous matter tends to reach very negative values of the mean energies, almost converging to similar values for all bins. The general behaviour of the luminous component resembles the behaviour of the most boundly tied particles of the collapse models. The main reason for this may be the fact that, after the initial interaction, the luminous component finds its equilibrium state within the deeper potential well of the dark halo. This might occur through a partial collapse of the luminous matter inside the dark halo. In the case of the dark matter component, there is also some violation of the ordering of the mean energies per bin. In fact, the initially most bound bins (number 1) cross upwards and gain energy in some cases. The halo seems to be the only system that actually shows this behaviour clearly.

The D models and the luminous component also present the same effect as seen in collapses: the particles initially more bound to the system tend to lose energy as a function of the initial orbital energy, as can be seen by the dashed line in the figure, which connects the most bound bins (1). For haloes, this behaviour is not as clear.

Note that the mean biding energy of the most bound bins remains at an almost constant value for collapses (see the dashed lines in Fig. 10), rising steeply for the 'hottest' collapses. The C models present more fluctuations in this behaviour. For mergers, on the other hand, these changes proceed more smoothly and systematically with the initial orbital energy (dashed lines in Fig. 11). This means that the initially most bound collection of particles remain on average the most bound particles after the relaxation, but at a more negative mean energy than the slower (less negative $E_{\rm orb}$) mergers.

It is clear that if the ordering of the mean energies of particles, partitioned at a coarse-grained level, is strictly conserved, as in collapses, then the most bound particles (on average closer to the barycentre) continue be the most bound particles after virialization. However, as pointed out previously, this ordering conservation *does not* occur for mergers. In other words, some complex behaviour seems to take place during the merger involving the more central or bound particles, an effect that *does not* occur at all in collapses (except for some small shuffling between the *less* bound bins for the 'hottest' C models). In summary, we entirely confirm the results of Kandrup et al. for collapses, but in the case of mergers, some violation of the ordering conservation of the energy bins is present.

4 DISCUSSION

We have simulated a hierarchical non-dissipative merger scheme similar to that of CdCC95; however, using different models to represent the progenitors of the first-generation mergers. In contrast with CdCC95, which considered King density profiles, we used models endowed with cuspy profiles, such as the Hernquist density profile. Also models with a dark halo second component were used in this study. A comparison with collapse simulations (previously analysed in DCdCR02 and extended here to include collapses with initial spins) is presented.

We found that the one-component Hernquist mergers give results similar to those found by CdCC95 for the one-component King models, namely both were able to build up small-scattering FP-like correlations with slopes consistent with those found for the near-infrared FP of nearby galaxies. The two-component models also reproduce a FP-like correlation, but with a significantly steeper slope that is in agreement with that found for galaxies at high redshift (Pahre 1998). Pahre finds that the slope of the near-infrared FP decreases with increasing redshift (see his fig. 7.2). Another important piece of evidence of the evolution of the FP with redshift comes from the work of Kelson et al. (1997). The authors find that the structure of the galaxies in the analysed sample has not changed significantly since $z = 0.58$, based on the fact that the observed scatter is rather low: ± 0.067 in $\log r_{\rm e}$. Besides, they find a dependence between M/L_V and the redshift, which reinforces the idea of a stellar population effect in the evolution of the FP.

In nature, dissipational effects must have played a role in producing the FP relations and their scatter, but it would be unwise to completely disregard the role of stellar dynamics in shaping ellipticals

as well. Our simulations are only of a dynamical character, with the M/L ratio being fixed by construction. Systematic non-homology in the evolved models can produce FP-like 'tilts' compatible with those found in nature. In particular, we show the importance of the gravitational potential of the halo for changing the 'tilt' of the FP: the magnitude of the change can be seen directly from a comparison between one- and two-component Hernquist merger models (cf. Fig. 1). In other words, this simple result clearly shows how the FP slope may be changed dynamically just by the addition of a halo. Therefore, our results suggest that the structure evolution of the halo could also have a collateral importance in changing and shaping the FP 'tilt', along with population evolution effects (e.g. Kelson et al. 1997). We speculate on the possibility that haloes may suffer evolution from $z \sim 0.5$ to the present. The evolution could be in the form of tidal stripping, which would decrease the mass of the halo, or by the presence of supermassive central black holes, which could alter the matter distribution of the halo, forming a core (cf. Hennawi & Ostriker 2002). If dark matter presents some level of self-interaction (cf. Spergel & Steinhardt 2000), then it may drive evolution towards a core in less than a Hubble time (cf. Yoshida et al. 2000). If some of these processes have operated in haloes during the past few Gyr, in the sense of altering their gravitational potentials at the centres of galaxies, the characteristic scaling properties of the luminous/baryonic component might have changed as well. Whether any of these possibilities are in fact true is at present an open issue.

A qualitative analysis of the behaviour of the mean energy of collections of particles (as advocated by Kandrup et al. 1993) leads us to consider the possibility that 'mesoscopic' constraints could have some connection to the central non-homology. The conservation of the ordering of the mean energy of collections of particles implies that the process of 'mixing' in the one-particle energy space is quite inefficient compared with 'mixing' in configuration and/or velocity space (see the discussion in Kandrup et al.). This seem to be true for collapses, but not entirely so for the central parts of mergers.

The most intense tidal perturbations (shocks) seem to be found for the most rapidly merging systems (more negative orbital energies). In this case, the particles probably withdraw the energy from the relative orbit of the merging pairs at one major fluctuation. Secondary fluctuations on the gravitational potential evolve afterwards rapidly and reach equilibrium in a short time-scale as well. The stratification of the kinetic energies resembles that of the progenitor in this case. On the other hand, if the orbital energy is less negative (slow mergers), there is some time for the particles to withdraw energy from the orbit of the pair, and this process involves periodic large fluctuations on the potential that evolve slowly, taking a larger amount of time to stabilize. This process may be important in 'heating up' the central parts of the models approaching $E_{\rm orb} \rightarrow 0$. This should be important in defining the non-homology in mergers because the stratification of the kinetic energies is indeed different from that of the progenitor.

On the other hand, in the case of collapses, the dynamics seem to operate in a different manner from in mergers. Collapses starts off from a spherically symmetric condition that mergers do not share. Collapses also produce not only fast by very high-amplitude gravitational potential fluctuations that dump rapidly. This process should be very efficient in heating up the central parts of the models in configuration and/or velocity space, but not efficient enough to have the particles 'forget' their initial energies in a collective ('mesoscopic') manner. As already pointed out by Kandrup et al., this behaviour is at odds with Lynden-Bell's theory of 'violent relaxation', where 'mixing' in energy space is not expected to be inefficient for any given collection of particles. At the same time, we have found that collapses seem to 'prefer' forming homologous systems, whereas mergers do not. Some connection between 'mesoscopic' constraints and non-homology seems to be apparent, but this is an open question.

We did not attempt at this time to rigorously try to connect the behaviour of the violation of the ordering of the energy bins (Figs 10 and 11) with the behaviour of the 'central' to 'envelope' kinetic energies (Figs 7 and 8). Although interesting, in order to fully understand this effect, we would need to probe the problem of relaxation in a much deeper and/or formal manner, which is not the objective of our paper at the present time. Figs 10 and 11 illustrate a diagnostic on the behaviour of the change of energy of the system owing to relaxation in a 'mesoscopic' scale. Figs 7 and 8 show a different diagnostic, where the change of energy of the central and external parts of the system are compared with their *progenitor models*, not to their initial condition (as in Figs 10 and 11), and hence refer to a more 'macroscopic' feature of the relaxation process. On the other hand, the main point of Figs 10 and 11 is *not* to show how the energy of collections of particles change owing to relaxation (although it also certainly shows that) but to *what degree* the ordering of their mean energies is violated. This type of analysis was first envisaged by Kandrup et al. in 1993 and is still not well understood. In our opinion, it is not at all clear how one could find any immediate connection between both sets of figures. We know that the non-homology is primarily a systematic function of $E_{\rm orb}$. Both sets of figures show systematic behaviour of two different types of diagnostics as a function of $E_{\rm orb}$. Collapses show almost no dependence of these same diagnostics with β (except for the 'hottest' collapses). Therefore, it seems that relaxation through merging embodies some mechanism that is effective in differentiating the final models, producing non-homology, whereas this mechanism is absent or highly precluded in collapses (again, except for the 'hottest' ones, which are just a small perturbation from equilibrium of the progenitor model). In fact, what is lacking in order to make any progress in this direction is a systematic understanding of the nature of the gravitational relaxation mechanism, where several conceptual issues are still unsolved (cf. Padmanabhan 1990).

In any case, our results seems to strengthen the idea that dissipationless merging could produce significant non-homology in the final objects and therefore FP-like relations in the same sense and with comparable values of the FP 'tilt' as those observed in ellipticals. We have shown that, on purely dynamical grounds, mergers can produce FP-like relations while *simple* collapses cannot (two-component collapses were not investigated here and will be a subject for future work). The evolution of gradients in the gravitational field of the merging galaxies seem to dictate the final non-homology of the end products. Further investigations are necessary in order to establish, quantify and rigorously explain these complex effects, as preliminary discussed in this paper.

ACKNOWLEDGMENTS

We thank J. Dubinski and R. Carlberg for useful discussions during this project. We also thank the anonymous referee for his/her constructive suggestions. CCD acknowledges fellowships from FAPESP under grants 96/03052-4 and 01/08310-1. ALBR acknowledges fellowships from FAPESP under grant 97/13277-6. This work was partially supported by CNPq, PRONEX-246 and Fapesp under grants 00/06695-0 and 00/06770-2.

REFERENCES

Aguilar L.A., Merritt D., 1990, ApJ, 354, 33
Barnes J., Hut P., 1986, Nat, 324, 446
Bekki K., 1998, ApJ, 496, 713
Bender R., Saglia R.P., 1999, in Merritt D.R., Valluri M., Sellwood J.A., eds, ASP Conf. Ser. Vol. 182, Galaxy Dynamics. Astron. Soc. Pac., San Francisco, p. 113 (astro-ph/9811416)
Binney J., 1982, MNRAS, 200, 951
Binney J., Tremaine S., 1987, Galactic Dynamics. Princeton Univ. Press, Princeton
Burkert A., 1995, ApJ, 447, L25
Busarello G., Capaccioli M., Capozziello S., Longo G., Puddu E., 1997, A&A, 320, 415
Capelato H.V., de Carvalho R.R., Carlberg R.G., 1995, ApJ, 451, 525 (CdCC95)
Capelato H.V., de Carvalho R.R., Carlberg R.G., 1997, in da Costa L.N., Renzini A., eds, Galaxy Scaling Relations, Origins, Evolution and Applications, Proc. from the ESO Workshop. Springer-Verlag, Berlin, p. 331
Carpintero D.D., Muzzio J.C., 1995, ApJ, 440, 5
Ciotti L., Lanzoni B., Renzini A., 1996, MNRAS, 282, 1
Dantas C.C., 2001, PhD thesis, Instituto Nacional de Pesquisas Espaciais, Brazil
Dantas C.C., Ribeiro A.L.B., Capelato H.V., de Carvalho R.R., 2000, ApJ, 528, L5
Dantas C.C., Capelato H.V., de Carvalho R.R., Ribeiro A.L.B., 2002, A&A, 384, 772 (DCdCR02)
Djorgovski S.G., 1988, in Thuan T.X. et al., eds, Proc. Moriond Astrophysics Workshop, Starbursts and Galaxy Evolution. Gif sur Yvette, Editions Frontières p. 549
Djorgovski S.G., Davis M., 1987, ApJ, 313, 59
Djogorvski S.G., Santiago B.X., 1993, in Danziger I.J., Zeilinger W.W., Kjar K., eds, Structure, Dynamics and Chemical Evolution of Elliptical Galaxies, Proc. ESO/EIPC Workshop, ESO Conf. and Workshop Proc. 45. ESO, Garching, p. 59
Dressler A., Lynden-Bell D., Burstein D., Davies R.L., Faber S.M., Terlevich R.J., Wegner G., 1987, ApJ, 313, 42
Dubinski J., 1988, MS thesis, Univ. of Toronto
Gebhardt K. et al., 2000, ApJ, 539, L13
Gerhardt O., Kronawitter A., Saglia R.P., Bender R., 2001, AJ, 121, 1936
Gott J.R., III, 1973, ApJ, 186, 481
Graham A., Colless M., 1997, MNRAS, 287, 221
Hennawi J.F., Ostriker J.P., 2002, ApJ, 572, 41
Hernquist L., 1990, ApJ, 356, 359
Hjorth J., Madsen J., 1995, ApJ, 445, 55
Kandrup H.E., Mahon M.E., Smith H., 1993, A&A, 271, 440
Kelson D.D., van Dokkum P.G., Franx M., Illingworth G.D., Fabricant D., 1997, ApJ, 478, L13
Kronawitter A., 2000, A&AS, 144, 53
Mihos J.C., Dubinski J., Hernquist L., 1998, ApJ, 494, 183
Navarro J.R., Frenk C.S., White S.D.M., 1997, ApJ, 490, 493
Padmanabhan T., 1990, Phys. Rep., 188, 285–362
Pahre M., 1998, PhD thesis, California Institute of Technology
Pahre M.A., Djorgovski, 1997, in Arnaboldi M., Da Costa G.S., Saha P., eds, ASP Conf. Ser. Vol. 116, The Nature of Elliptical Galaxies, Proc. 2nd Stromlo Symp. Astron. Soc. Pac., San Francisco, p. 154
Pahre M.A., Djorgovski S.G., de Carvalho R.R., 1998, AJ, 116, 1591
Peebles P.J.E., 1971, A&A, 11, 377
Renzini A., Ciotti L., D'Ercole A., Pellegrini S., 1993, ApJ, 419, 52
Salucci P., Burkert A., 2000, ApJ, 537, L9
Siopis C., Sideris I.V., Pogorelov I.V., Kandrup H.E., 2000, in Ossipkov L.P., Nikiforov I.I., eds, Proc. Int. Conf. on Stellar Dynamics, Classical to Modern, St Petersburg Univ. Press, pp. 420–426 (astro-ph 0010326)
Spergel D.N., Steinhardt P.J., 2000, Phys. Rev. Lett., 84, 3760
Walker I.R., Mihos J.C., Hernquist L., 1996, ApJ, 460, 121
Wilkinson A., James R.A., 1982, MNRAS, 199, 171
Yoshida N., Springel V., White S.D.M., Tormen G., 2000, ApJ, 544, L87

This paper has been typeset from a TEX/LATEX file prepared by the author.